Proceedings of the
Annual Stability Conference
Structural Stability Research Council
San Antonio, Texas, March 19-22, 2024

Deformation analysis of solar photovoltaic (PV) structures: lateral-torsional buckling of C purlins restrained by solar modules

Xinlong Du[1], Tracy Becker[2]

Abstract
Solar photovoltaic (PV) structures such as canopies and fixed-tilt racking structures may experience large deformations under wind loading. The nonlinear responses of these structures are quite complicated considering that cold-formed C sections, Z sections and Hat sections are widely used. To accurately capture the behavior of these nonsymmetric sections, the effects of axial-flexural-torsional interaction and warping should be considered. In this research, these sections are modeled using a displacement-based beam element within the OpenSees corotational framework. Axial-flexural interaction is accounted for through corotational transformation. Warping, flexural-torsional, and axial-torsional interactions are included in the element formulation in the basic system that is corotating with the beam element chord. Nonlinear responses of the purlin-module joints are modeled using nonlinear springs that can simulate the effects of friction, slipping, and bearing. The analysis focuses on lateral-torsional buckling (LTB) of C purlins of PV structures, where the effects of the purlin-module joints on the LTB capacity are investigated. The results show that if the purlin-module joints are fully restrained or modeled as nonlinear springs (approximating a top-down clamp joint), LTB is delayed until yielding of the purlins. If the purlin-module joints are pin connections, the LTB capacity is still higher than the LTB capacity of an unbraced purlin.

1. Introduction

As a strategy to reduce carbon emission and mitigate climate change, we are experiencing and expecting significant increase in construction and reliance on solar power as a green energy solution. According to the *Solar Futures Study* (SETO 2021) released by the US Department of Energy, solar power would need to expand from currently providing 5% of the US electricity to 40% by 2035 and 45% by 2050. To expedite the deployment of solar power, the Levelized Cost of Electricity generated by utility-scale photovoltaic (PV) needs to be reduced. Consequently, the design of the solar racking systems is of great importance as the same design may be repeated thousands of times in the construction of a large solar farm, which means a small increase in structural member size may result in a huge amount of material cost. As the solar racking systems are relatively new structures, there are not enough research on the behaviors of these structures

[1] Postdoctoral Scholar, University of California, Berkeley, <xinlongdu@berkeley.edu>
[2] Associate Professor, University of California, Berkeley, <tcbecker@berkeley.edu>

under natural hazards, and therefore there are currently no widely accepted design standards that can guarantee resilience of the PV structure and at the same time help engineers to select the smallest structural members. This paper focuses on the analysis and design of solar PV structures and aims to accurately predict the buckling capacity of purlins connected by solar modules.

Solar modules are usually mounted to flat roofs or grounds through different racking systems. The commonly used ground-mounted racking systems include fixed-tilt single-post or dual-post structures, canopies, and single-axis trackers. For the fixed-tilt or canopy PV structures, a set of solar modules are usually mounted to purlins, which are connected to beams/rafters and then to posts. The purlins are usually made of cold-formed C sections or Z sections, while vendors may use a lot of different sections (e.g., Hat, HSS, W, and pipe) for beams/rafters and posts. Fig. 1 shows a typical fixed-tilt dual-post solar PV structure, where two rows of PV modules are in portrait position. For each row, discrete PV modules are mounted on two long parallel C purlins at the longer side of modules. Rafters are Hat sections, while posts and braces are pipe sections.

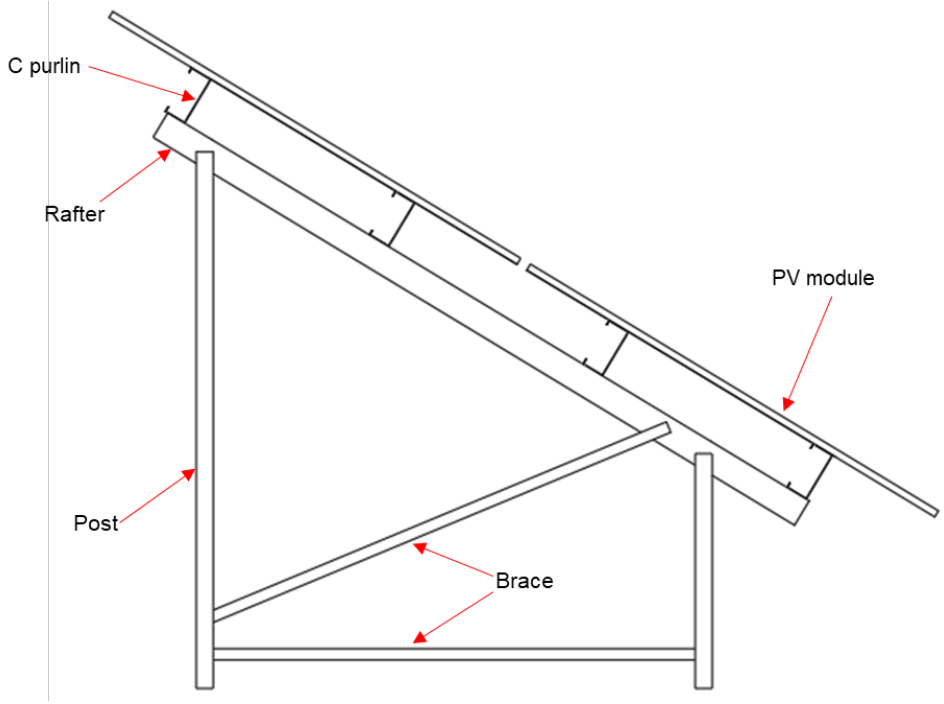

Figure 1: A typical dual-post solar PV structure

There are no reliable connections between adjacent modules; therefore, the rigid diaphragm action, which is a common assumption in buildings, is not applicable due to discontinuity of modules. When designing the purlins for lateral-torsional buckling (LTB), determining the unbraced length is of significant importance. Based on our survey with several engineers, most agree that the unbraced length should be the span between rafters and the bracing effects of modules should be neglected; however, they note that in practice many engineers consider the module connections as brace points, and thus use the module width as the unbraced length. These different choices lead to a large difference in the design of purlins. Therefore, this paper tries to do large deformation analysis of PV structures, where LTB of purlins can be captured and the bracing effects of modules can be quantified. The results of this study aim to help structural engineers select appropriate sections for purlins while considering the bracing effects of modules.

2. Structural subassembly for study

For the current study, a subassembly of two parallel purlins with six modules is taken from the prototype structure in Fig. 1. A schematic of the subassembly is shown in Fig. 2, where PV modules are mounted on purlins at the quarter point and three-quarter point of the longer side of modules. The length of the two purlins is 262.56 in. The size of the modules is 84 in by 41.26 in, and the spacing between modules is 1.0 in. A PV module is made of the peripheral aluminum module frame and the module laminate in the middle that consists of layers of thin glass, encapsulant, and solar cells. The normal thickness of the module laminate is around 4 to 5 millimeters, and it needs to be mounted to module frames for higher stiffness and strength. A schematic of the joints between modules and purlins is shown in Fig. 3. The one in Fig. 3(a) is an interior joint shared by two adjacent modules, where a top-down clamp is used with a bolt to attach module frames to the top flange of the purlin. If the top-down clamp is used for the joints at the edge of the subassembly, the configuration will be similar, but the only difference is that the clamp only has one arm. The one in Fig. 3(b) is a though bolt joint, where the bottom lip of the module frame is directly bolted to the top flange of the purlin.

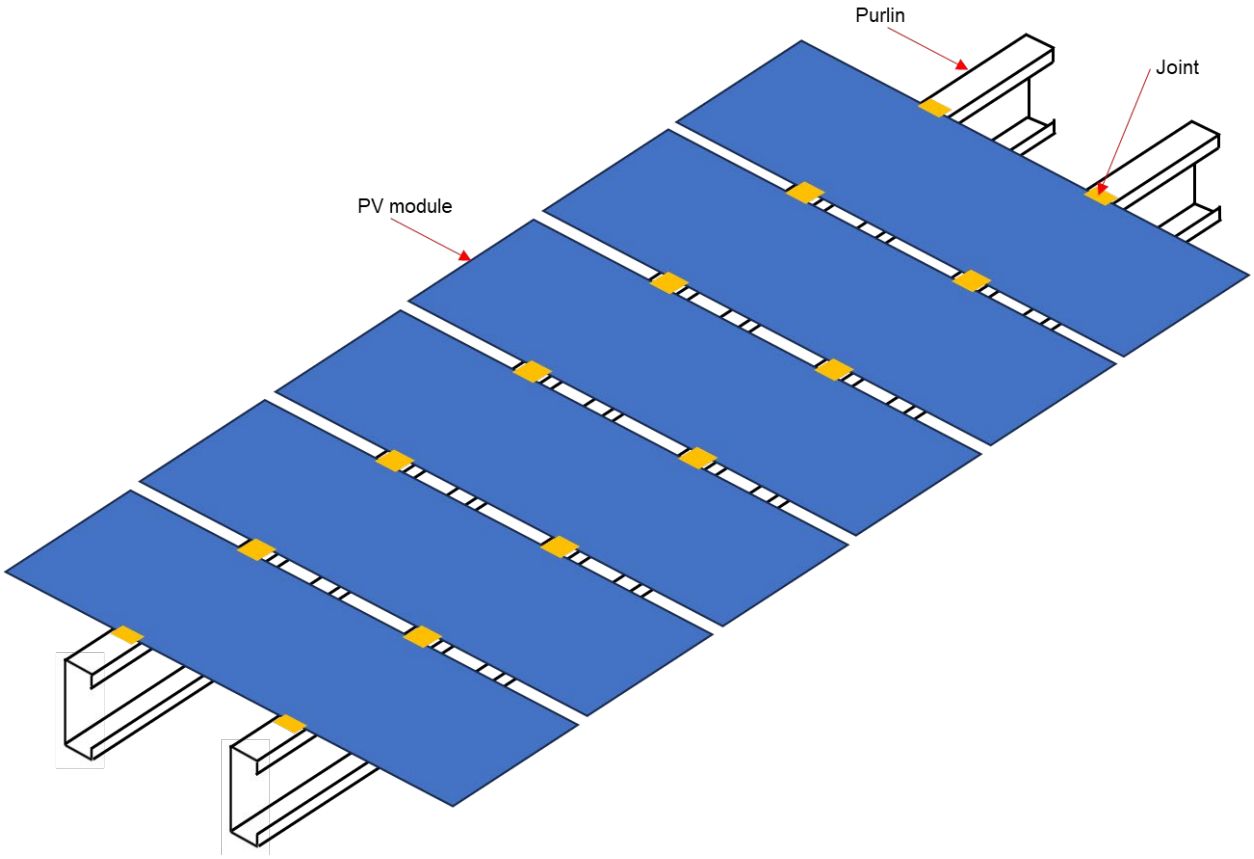

Figure 2: Structural subassembly with two C purlins and six solar modules (not to scale)

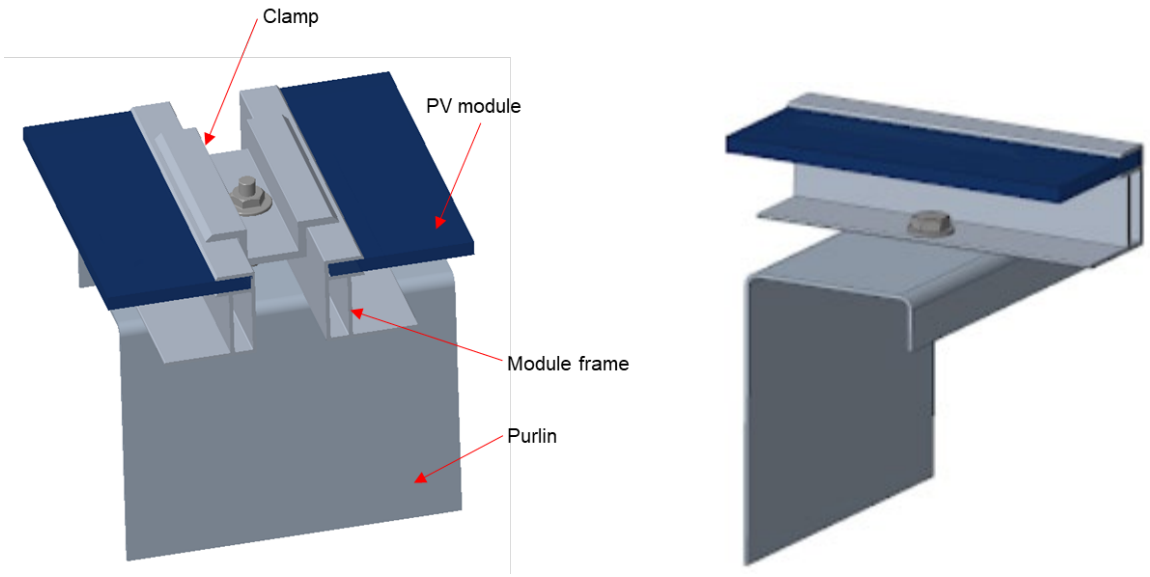

(a) Top-down clamp (b) Module lip through bolt

Figure 3: Examples of purlin-module joints

PV modules including module frames and module laminates are often provided by module manufacturers, while purlins and purlin-module joints need to be designed by structural engineers. After obtaining the required bending moments through structural analysis, the purlins are designed one by one. Here, we focus on the limit state of LTB of purlins. The available strength of a purlin depends on its unbraced length. To investigate the supporting effects from modules and the other purlin in this subassembly, finite element models will be built in the following sections and large deformation analysis will be run to estimate the capacity of the purlins with modules.

3. Effects of purlin-module joints on the LTB capacity: fully restrained and pin joints

In this section, the purlins are C sections with lips with a size of 8CS2.5x0.059 in, whose properties can be found in AISI manual for Cold-Formed Steel Design (AISI 2002). The yield strength of the purlins is 55 ksi. The two purlins are simply supported and only bending moments are applied to each end of the two purlins with opposite directions, which means that the moment gradient factor Cb for LTB is 1.0. The analytical model is displayed in Fig. 4, where the purlins are modeled as displacement-based beam elements with fiber sections developed by Rinchen et al. (2022). The element is implemented in the OpenSees corotational framework (Mckenna et al. 2010). In this element, axial-flexural interaction is accounted for through corotational transformation. Warping, flexural-torsional, and axial-torsional interactions are considered in the element formulation in the basic system that is corotating with the beam element chord. The reference axis of this element is the shear center axis. Consequently, the boundary conditions at the two ends of the purlins are applied to the shear center, which is reasonable since usually the web instead of the bottom flange of the purlins is connected to rafters using bolts and angles. We assume the modules are mounted to the middle of the purlin's top flange; therefore, a horizontal and a vertical rigid offset are used to connect the purlin and module frame at the middle of the purlin's top flange (see Fig. 4). The uniaxial bilinear Steel01 material in OpenSees is used with a 0.001 strain hardening ratio for each fiber of the purlins. The typical cross-section height of the module frames is 32 mm, while the widths of the top and bottom flanges of the module frames are about 12 mm and 33 mm, respectively. The module frames are modeled as elastic beam elements developed by Rinchen et

al. (2016) and also implemented in the OpenSees software. The interactions between two adjacent modules are neglected. The module laminate (i.e., the combination of layers of thin glass, encapsulant, and solar cells) is neglected in structural analysis because: 1) it is very thin (usually <5 mm) compared to the cross-section height of the structural members (32 mm for module frames and 200 mm for purlins); 2) the analysis in the following sections shows that the module frames can provide enough support to prevent LTB of purlins if the joints between module frames and purlins have enough stiffness, which means we do not need the stiffness of the module laminate.

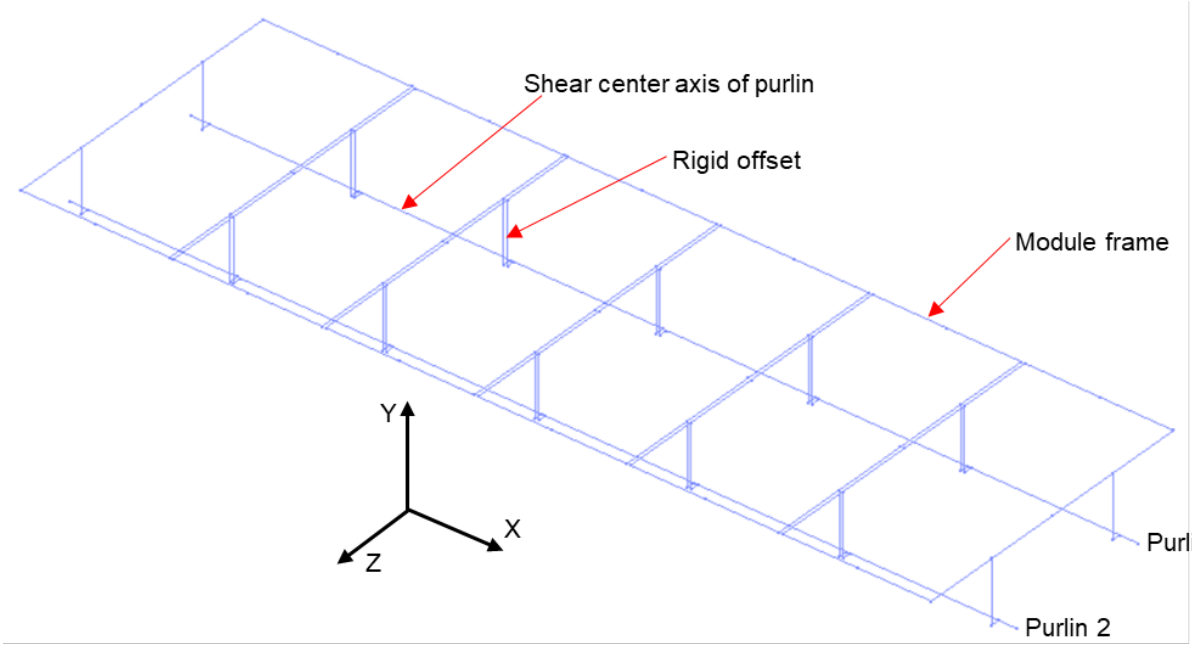

Figure 4: Analytical model of the subassembly in OpenSees screen (not to scale)

3.1 Fully restrained purlin-module joints

In this section, we assume that the purlin-module joints are fully restrained, and we want to obtain the capacity of the two purlins under uniform bending through quasi-static analysis. We first apply a small torque (Mx) at the midspan of each purlin as initial imperfections. We then apply the bending moments about Z axis (Mz) at the two ends of each purlin. The applied moment at one end of a purlin has the same magnitude but oppositive direction as the moment at the other end of the purlin. We have run two cases: the top flange of the purlins under compression and the top flange of the purlins under tension. We know that the post-buckling behavior of a single C purlin is different for different directions of the initial twist; therefore, for each case we also explore the effects of positive and negative initial torque Mx. Exactly the same external bending moments and torque are applied to the two purlins. The relationship between the applied moment and the twist at midspan is shown in Fig. 5 and Fig. 6 for the two cases, respectively. The yield strength and critical buckling load for LTB are from the AISI manual. The responses of a single purlin without panels obtained using the displacement-based beam element are also plotted for comparison and validation. It is seen that the LTB capacity from nonlinear analysis of the single purlin matches well with the critical buckling load for LTB from the AISI manual, and that the post-buckling stiffness for positive initial twist is higher than that for negative initial twist. Importantly, Fig. 5 and Fig. 6 show that the capacities of purlins for both cases are slightly higher than the yield strength of the purlin, which means that module frames can delay LTB of purlins. Fig. 7 shows a

deformed shape of the subassembly when the applied moment is about 78 kip-in. It is seen from Fig. 7(b) that the purlins do not have large lateral displacements, which means that LTB is restrained to some extent. Specifically, at this load level the vertical displacement at midspan is 3.1 in, while the lateral displacement at midspan is 0.2 in. Fig. 5 shows that inelastic LTB happens after the applied moments are greater than the yield strength. At the end of the analysis, the vertical displacement at midspan is approximately 5.2 in, while the lateral displacement at midspan is approximately 1.4 in.

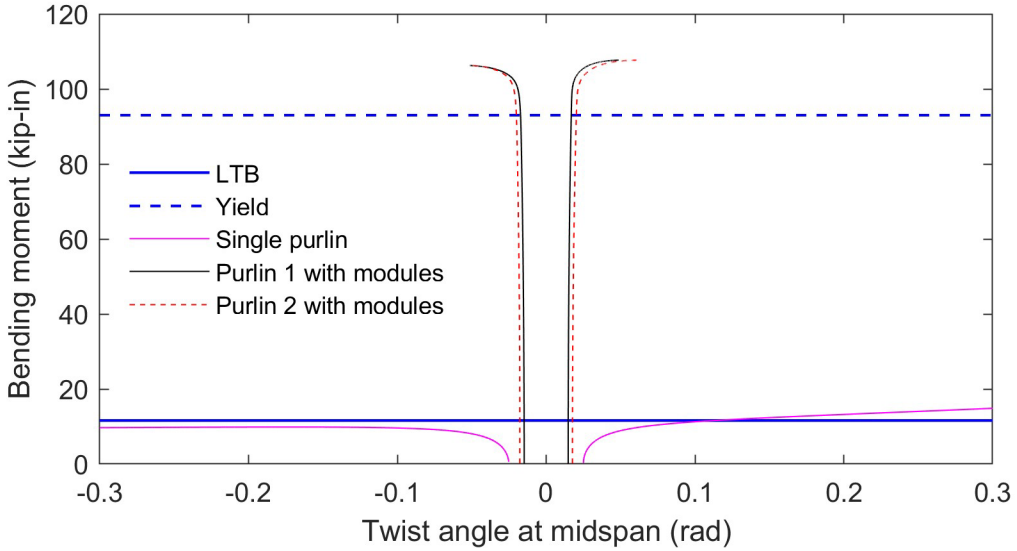

Figure 5: Moment-midspan twist plots of the purlins with top flanges under compression (fully restrained purlin-module joints)

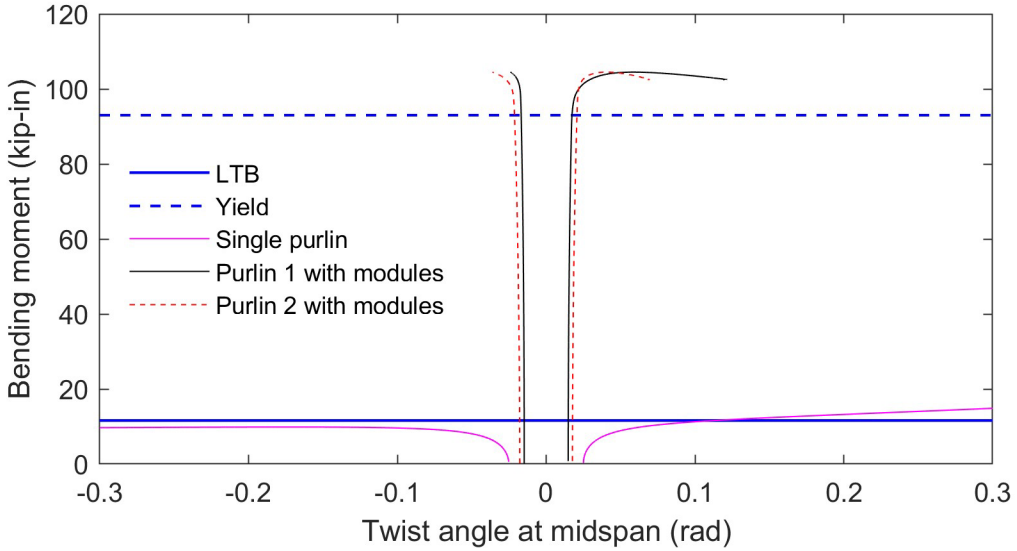

Figure 6: Moment-midspan twist plots of the purlins with top flanges under tension (fully restrained purlin-module joints)

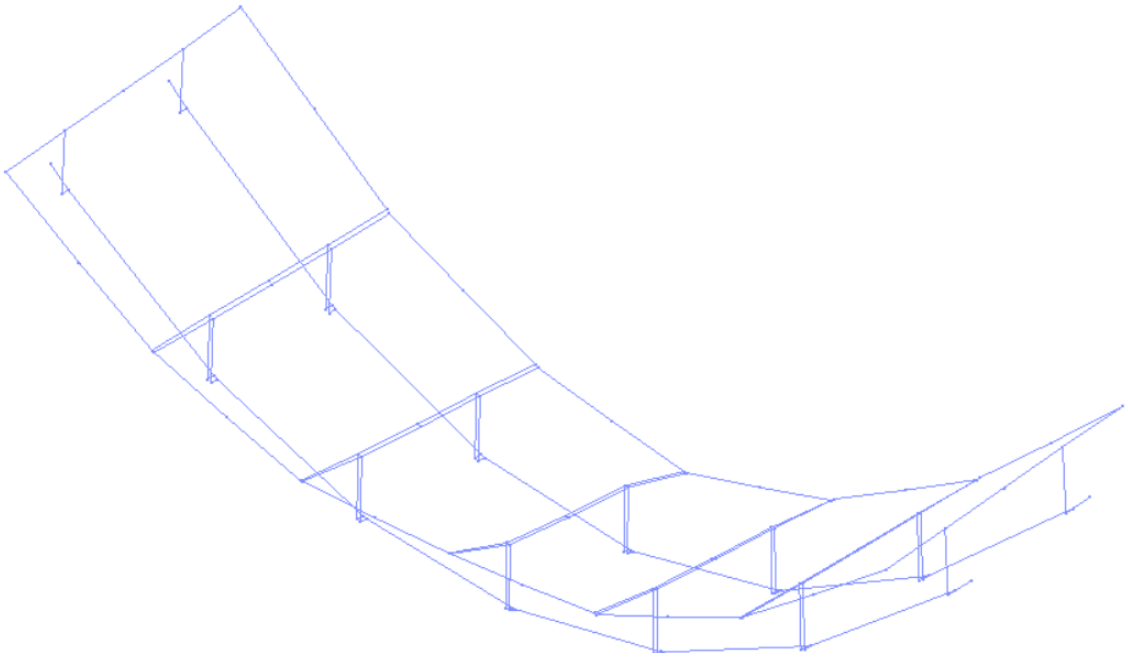

(a) 3D deformed shape (not to scale)

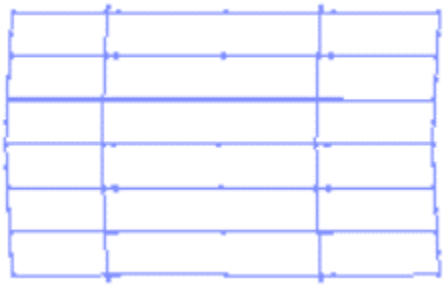

(b) Plan view of the deformed shape (not to scale)

Figure 7: Deformed shape for the case of the top flanges of purlins under compression (fully restrained purlin-module joints, negative initial twist)

3.2 Pin purlin-module joints

In this section, we assume that the purlin-module joints are pin connections, and we apply the same boundary conditions and loads as in Section 3.1. In this case, the twist of the purlins cannot be restrained by the module frames; therefore, we expect the capacity of the purlins will be lower than the case of fully restrained purlin-module joints. It is seen from Fig. 8 and Fig. 9 that the capacities of the purlins are in the range of 60 to 70 kip-in, which is smaller than the yield strength but still significantly greater than the LTB capacity of a single purlin. This means that LTB of purlins can be partially restrained by module frames even with pin purlin-module joints. Considering the deformed shape of a purlin after LTB, we think that there are two ways to restrain LTB: 1) restrain twist of the purlin; 2) restrain lateral displacement of the purlin. Module frames with pin purlin-module joints can restrain LTB through the second way. This is because during LTB of purlins, the two long sides of a module frame will have a difference in lateral displacement, which will force the module frame to deform from a rectangle to a parallelogram. Therefore, module frames can provide some lateral support to purlins with the prerequisite that the joints between the four members of the module frames can transfer moments. This explanation can be verified by the deformed shape shown in Fig. 10 for the case of the top flanges of purlins under tension. It is seen

in Fig. 10(b) that the deformed shape of a module frame becomes a parallelogram. At the end of this analysis, the vertical displacement at midspan is approximately 3.4 in, while the lateral displacement at midspan is approximately 4.8 in.

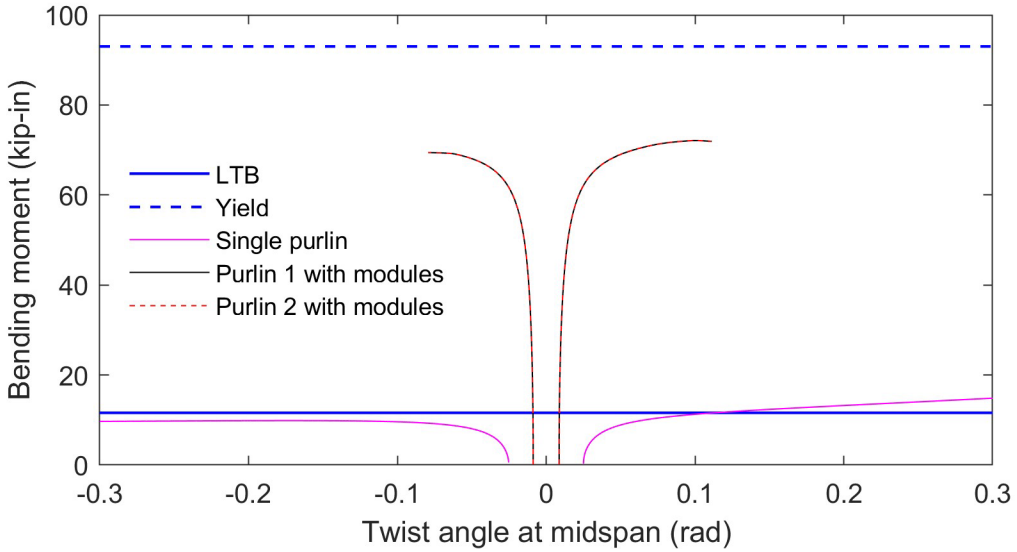

Figure 8: Moment-midspan twist plots of the purlins with top flanges under compression (pin purlin-module joints)

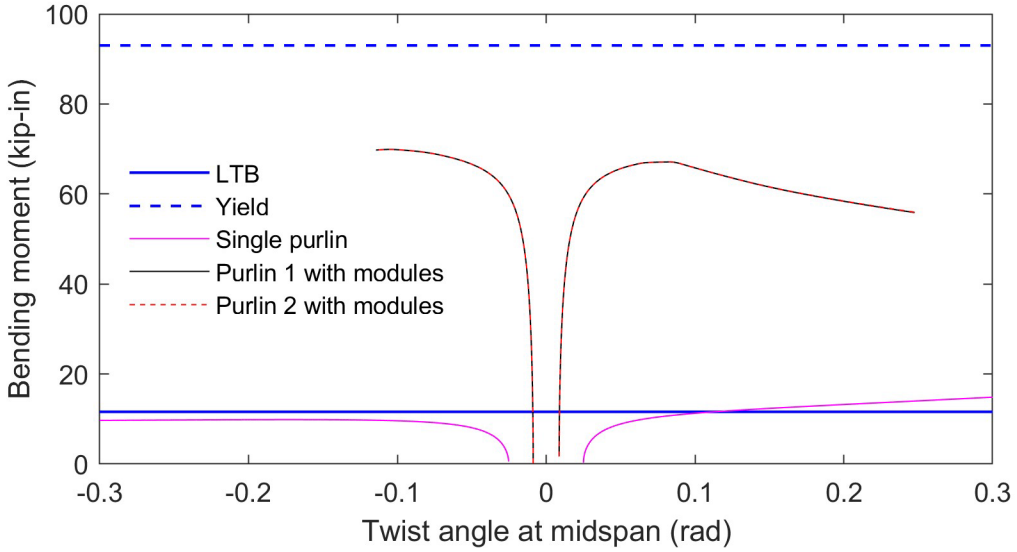

Figure 9: Moment-midspan twist plots of the purlins with top flanges under tension (pin purlin-module joints)

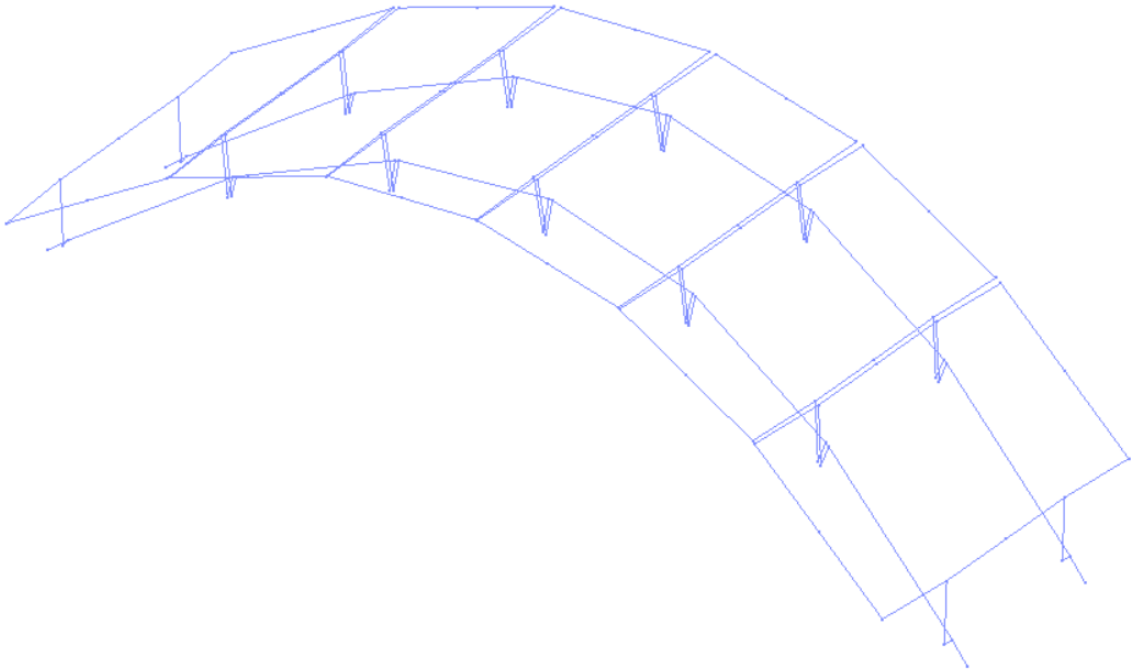

(a) 3D deformed shape (not to scale)

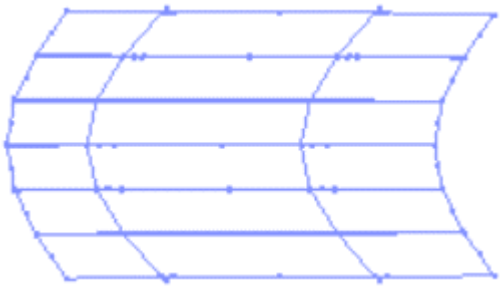

(b) Plan view of the deformed shape (not to scale)

Figure 10: Deformed shape for the case of the top flanges of purlins under tension (pin purlin-module joints, positive initial twist)

4. Effects of purlin-module joints on the LTB capacity: nonlinear spring models for joints

The purlin-module joints in reality are neither fully restrained nor pinned. In this section, we focus on the purlin-module joints with top-down clamps and use nonlinear springs to capture their behavior. We want to see the LTB capacity of purlins when we have this more accurate spring model for the purlin-module joints. The parameters of the springs are developed from an Abaqus model (see Fig. 11) using solid elements (Dassault Systemes 2017). Even though a clamp is shared by two modules, the joint in Fig. 11 is modeled as two separate joints in OpenSees as shown in Fig. 4. Each joint in OpenSees is represented by six nonlinear springs. Each spring is for one degree of freedom, which is developed by moving the module frame in the Abaqus model in the corresponding direction and recording the structural responses. The effects of friction, slipping, and bearing are included in the Abaqus analysis and therefore in the developed spring models. For simplicity, the interactions between two adjacent modules and the interactions between different degrees of freedom within one joint are not considered. As an example, the springs for displacement in the Z direction and rotation in the X direction are shown in Fig. 12. In OpenSees, the springs are modeled as ZeroLength elements with several parallel uniaxial materials, which are then inserted between module frames and the ends of the rigid offsets.

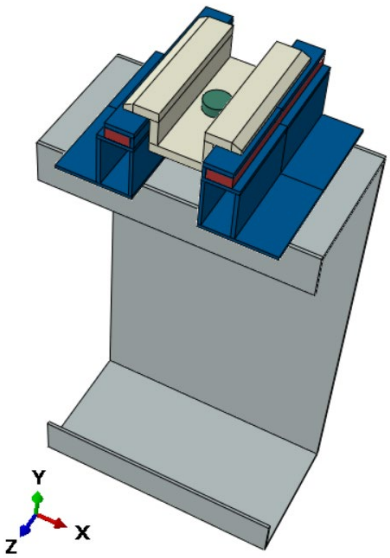

Figure 11: An Abaqus model of the purlin-module joints with top-down clamps

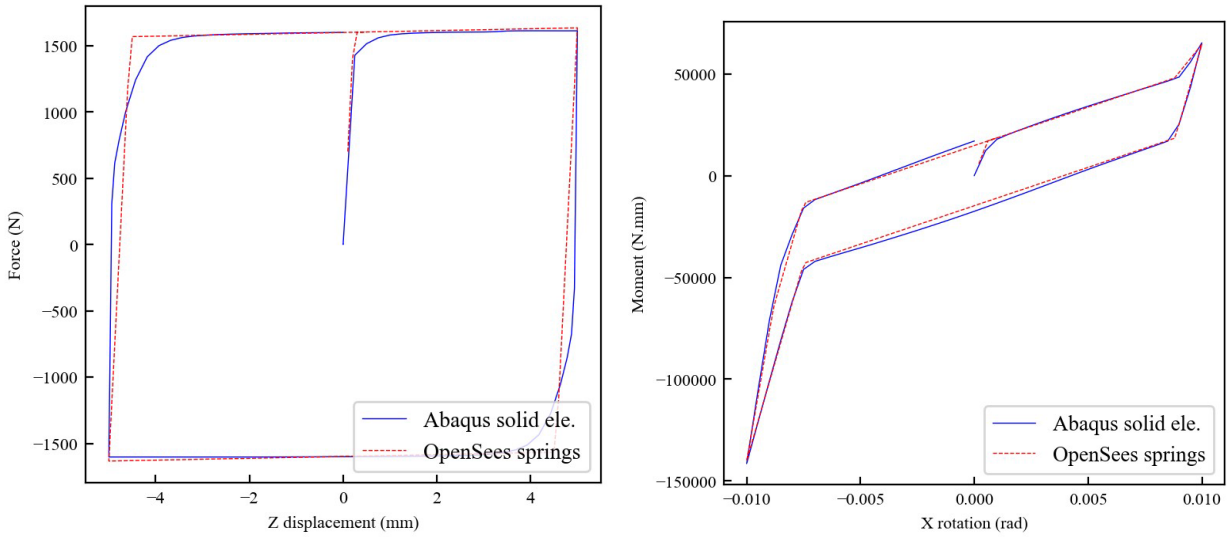

Figure 12: Response of OpenSees springs and Abaqus model

The element developed by Rinchen et al. (2020) has seven degrees of freedom at each node with the seventh degree of freedom accounting for warping. However, this seven-degree-of-freedom element is not compatible with other six-degree-of-freedom elements in OpenSees including the ZeroLength element we want to use to model the joints. In order to explore the effects of the semi-rigid joints on LTB of purlins, we use the six-degree-of-freedom element developed by Du and Hajjar (2021) to model the purlins, which is able to model LTB but cannot consider warping. Therefore, in this section, we change the purlin size to a C section that is not prone to warping. Specifically, we use section 3.94CS1.97x0.138 in with a lip of 0.650 in, which is not a standard C section in the AISI manual. For this C section with a length of 262.56 in, the critical buckling loads with and without considering warping are 14.6 kip-in and 13.9 kip-in, respectively, according to Trahair (1993). The error without considering warping is smaller than 5 percent. Therefore, it is reasonable to use the element developed by Du and Hajjar (2021) to model this purlin.

We use the same boundary conditions and external loads as in Section 3, but we just run the case of top flanges of purlins under compression with a negative initial torque. We perform the analysis for three different models for the purlin-module joints: fully restrained, pin, and nonlinear springs. The moment-twist responses for each joint model are shown in Fig. 13 to Fig. 15. The results of a single purlin analysis show that the critical load for elastic LTB can be accurately captured by the element. Fully restrained purlin-module joints can delay LTB until yielding. Using pin purlin-module joints can slightly increase the LTB capacity of the purlin but not as much as the purlin used in Section 3, which is probably due to that the height of the C section used in this section is much smaller the height of the C section used in Section 3 and smaller section height will lead to smaller lateral displacement of the purlin flange with the same twist. Fig. 15 shows that the nonlinear purlin-module joints can also delay LTB until yielding; however, the post-buckling stiffness is smaller than the case of using fully restrained joints (compared with Fig. 13).

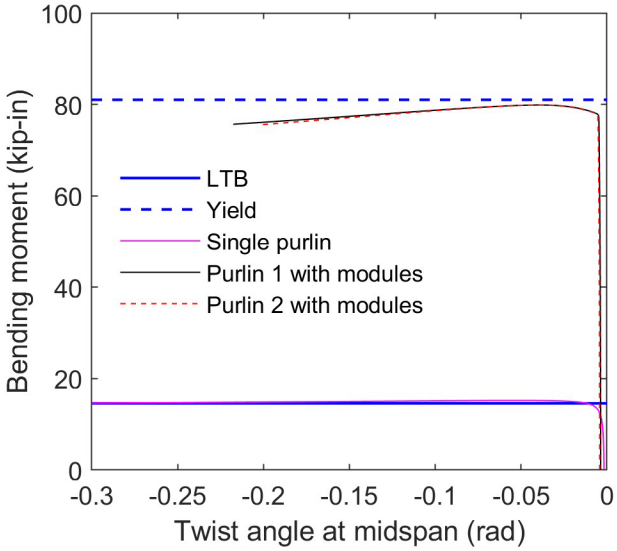

Figure 13: Moment-midspan twist plots of the purlins with top flanges under compression (no warping, fully restrained purlin-module joints)

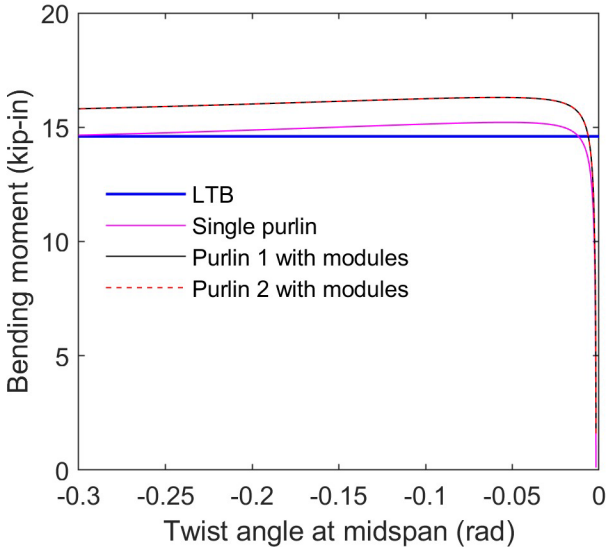

Figure 14: Moment-midspan twist plots of the purlins with top flanges under compression (no warping, pin purlin-module joints)

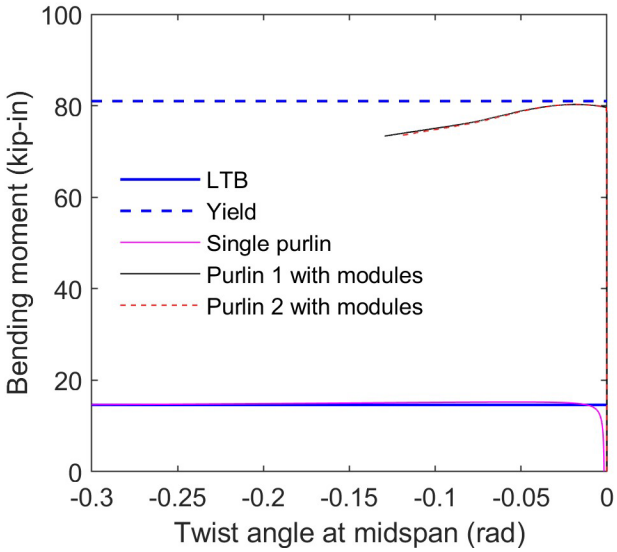

Figure 15: Moment-midspan twist plots of the purlins with top flanges under compression (no warping, nonlinear purlin-module joints)

5. Conclusions

To investigate the LTB behavior of C purlins supported by solar modules, a set of nonlinear finite element analyses are done with three different models for the purlin-module joints: fully restrained joints, pin joints, and nonlinear springs. Both geometric and material nonlinearities are considered in the analyses. The results show that both the fully restrained joints and nonlinear springs can delay LTB until yielding of purlins. Compared to a single purlin, purlins with pin purlin-module joints have higher LTB capacity, while the increase in the LTB capacity may depend on the height of the purlin section. In this work, the purlins are under uniform bending by applying moments at their ends. However, in reality loads are first applied to modules then transferred to purlins through the joints, which means the behavior of the purlin-module joints may be different from what is modeled in this paper. Consequently, further numerical or experimental research may be needed.

Acknowledgments

The material is based upon work supported by the US Department of Energy, Solar Energy Technologies Office. This support is gratefully acknowledged. Any opinions, findings, and conclusions expressed in this material are those of the authors and do not necessarily reflect the views of the sponsors.

References

American Iron and Steel Institute. (2002). "Cold-Formed Steel Design." Produced by Computerized Structural Design, S.C. Milwaukee, Wisconsin.

Dassault Systemes. (2017). "Abaqus 2017 Documentation." Dassault Systemes Simulia Corporation.

SETO. (2021). "Solar Futures Study". U.S. Department of Energy Solar Energy Technologies Office.

Du, X. and Hajjar, J. (2021). Three-dimensional nonlinear displacement-based beam element for members with angle and tee sections. *Engineering Structures*, 239, 112239.

McKenna F., Scott M.H., Fenves G.L. (2010). "Nonlinear finite-element analysis software architecture using object composition." *Journal of Computing in Civil Engineering*, 24 (1), 95–107.

Rinchen, Hancock, G.J., and Rasmussen, K.J.R. (2016). "Formulation and implementation of general thin-walled open-section beam-column elements in OpenSees." *Research Report R961*, The University of Sydney, Australia.

Rinchen, Hancock, G.J., and Rasmussen, K.J.R. (2020). "Geometric and material nonlinear analysis of thin-walled members with arbitrary open cross-section." *Thin-Walled Structures*, 153, 106783.

Trahair, N.S. (1993). "Flexural-Tortional Buckling of Structures." Boca Raton. CRC Press.